Available online at www.sciencedirect.com
SCIENCE DIRECT®
Journal of the European Ceramic Society 25 (2005) 949–956
www.elsevier.com/locate/jeurceramsoc

Synthesis, characterization, and electrical conduction of 10 mol% Dy_2O_3-doped CeO_2 ceramics

Yarong Wang [a,*], Toshiyuki Mori [a], Ji-Guang Li [b], John Drennan [c]

[a] *Eco-Materials Research Center, National Institute for Materials Science, Namiki 1-1, Tsukuba, Ibaraki 305-0044, Japan*
[b] *Advanced Materials Laboratory, National Institute for Materials Science, Namiki 1-1, Tsukuba, Ibaraki 305-0044, Japan*
[c] *Centre for Microscopy and Microanalysis, The University of Qeensland, St. Lucia, Brisbane, Qld 4072, Australia*

Received 8 November 2003; received in revised form 8 January 2004; accepted 18 January 2004
Available online 20 June 2004

Abstract

Well-densified 10 mol% Dy_2O_3-doped CeO_2 (20DDC) ceramics with average grain sizes of ∼0.12–1.5 μm were fabricated by pressureless sintering at 950–1550 °C using a reactive powder thermally decomposed from a carbonate precursor, which was synthesized via a carbonate coprecipitation method employing nitrates as the starting salts and ammonium carbonate as the precipitant. Electrical conductivity of the ceramics, measured by the dc three-point impedance method, shows a V-shape curve against the average grain size. The sample with the smallest grain size of 0.12 μm exhibits a high conductivity of $\sim 10^{-1.74}$ S/cm at the measurement temperature of 700 °C, which is about the same conduction level of the micro-grained 10 mol% Sm_2O_3- or Gd_2O_3-doped CeO_2, two leading electrolyte materials.

Keywords: CeO_2; Powder-chemical preparation; Electrical conductivity; Grain size

1. Introduction

Ceria (CeO_2) is a fluorite-structured ceramic material (space group Fm3m) that can be readily doped with a variety of aliovalent (alkaline-earth or rare-earth) cations to form solid solutions. When so doped, oxygen vacancies are introduced into the CeO_2 lattice for charge compensation and the materials become good ionic conductors for a variety of electrical applications. Rare-earth doped ceria has been considered promising electrolyte materials for application in solid oxide fuel cells (SOFCs) operating at intermediate temperatures (400–700 °C).[1,2]

The ionic conductivity of rare-earth doped ceria largely depends on the dopant type and dopant concentration, since the tendency of defect clustering (the formation of pairs between oxygen vacancies and the dopant cations) and the association energy of the clusters are both dopant size and concentration dependent.[3] Besides, microstructure of the sintered body is also known to have significant effects on the ionic conductivity. For the electrolytes with average grain sizes of several microns and above, improved electrical conduction along with an increase in the grain size was frequently observed, which was considered to be due to the decreased grain boundary density and can be well interpreted by the application of the brick layer model.[4–6] On the other hand, the electrical behavior of doped-ceria ceramics with much smaller grains of submicron or nano-size has only sparsely been investigated, mainly due to the lack of well sinterable powders and hence the difficulties encountered in sample preparation. The powders made via the traditional solid state reaction method need high sintering temperatures of ∼1700–1800 °C[7,8] to achieve the densities acceptable for practical applications. While the powders produced via wet-chemical routes (typically oxalate coprecipitation,[9,10] sol–gel,[11] and hydrothermal treatment[12,13]), though show improved reactivity compared to those via solid state reaction, still require typical sintering temperatures of 1400–1500 °C to achieve ∼99% of the theoretical, leading to ceramics of micron-sized grains. Such high fabrication temperatures leave very little opportunity for microstructure manipulation of the sintered bodies.

A careful survey of the previous reports indicates that the poor sinterability of the powders mainly arises from hard aggregation, large particle size, and irregular particle shape.

* Corresponding author. Tel.: +81-298-51-3354x8540; fax: +81-298-52-7449.
E-mail address: wang.yarong@nims.go.jp (Y. Wang).

0955-2219/$ – see front matter © 2004 Elsevier Ltd. All rights reserved.
doi:10.1016/j.jeurceramsoc.2004.01.020

Coprecipitation is a relatively convenient method among wet-chemical methods for powder preparation, and it is well recognized that the characteristics and sinterability of the resultant powders strongly depend on the type of starting salts and precipitant as well as synthesis conditions. We have used a carbonate coprecipitation method with ammonia carbonate as precipitant to overcome the above mentioned problems, and highly sinterable powders of 10 mol% Dy_2O_3-doped ceria (20DDC), which can be densified with high density via pressureless sintering at a very low temperature of ~950 °C, have been obtained via thermal decomposition of the carbonate precursors at suitable temperatures. Such a low sintering temperature allows us to tune the grain size of the resultant ceramics via varying the fabrication temperature and to investigate the relationship between electrical conduction and the average grain size.

2. Experimental procedure

2.1. Powder synthesis

The cation sources for the synthesis of 20DDC powders were cerium and dysprosium nitrate hexahydrates ($RE(NO_3)_3{\cdot}6H_2O$, RE = Ce and Dy), and ammonium carbonate ($(NH_4)_2CO_3$) was used as the precipitant. The chemicals were >99.5% pure and were all purchased from Kanto Chemical Co. Inc., Tokyo, Japan.

For precursor synthesis, 300 ml of the mixed salt solution (0.12 M for Ce^{3+} and 0.03 M for Dy^{3+}) was dripped into an equi-volume of the precipitant solution (1.5 M) kept at 70 °C under mild stirring. The resultant suspension, after aging at the reaction temperature for 1 h, was filtered via suction filtration. The precipitate cake was washed repeatedly with distilled water and finally rinsed with anhydrous alcohol (except those for chemical analysis and DTA/TG) before drying at room temperature with flowing nitrogen gas for more than 24 h. The dried precipitate cake was lightly pulverized with a zirconia mortar and pestle and then calcined in a tube furnace under flowing O_2 gas (50 ml/min) to yield oxide powders, using a heating rate of 5 °C/min and a residence time at the calcination temperature of 2 h.

2.2. Powder characterization

Compositions of the precursors were determined via chemical analysis. Cation contents were determined by the inductively coupled plasma (ICP) spectroscopic method with an accuracy of 0.01 wt.%; carbon contents were assayed on a simultaneous carbon/sulfur determinator with a detection limit of 0.01 wt.% (Model CS-444LS, LECO, St. Joseph, MI, USA); NH_4^+ contents were determined by the distillation-titrimetric method with an experimental error of ±0.1 wt.%; NO_3^- contents were analyzed by the spectrophotometric method on a Ubest-35 spectrophotometer (Japan Spectroscopic Co., Ltd., Tokyo, Japan) with a detection limit of 0.01 wt.%.

Differential thermal analysis/thermogravimetry (DTA/TG) of the dried precursor was made on a TG-DTA analyzer (EXSTASR6200, SEIKO, Tokyo, Japan) in flowing air (200 ml/min) with a heating rate of 10 °C/min, using platinum crucible as the sample container and alpha alumina as the reference.

Phase identification was performed via X-ray diffractometry (XRD) on a Rigaku RINT 2200HF$^+$ Ultima$^+$ X-ray diffractometer (Rigaku, Tokyo, Japan) operating at 40 kV/40 mA using monochromatized Cu Kα radiation. Diffractions were recorded in the range of $2\theta = 20$–120° by step scanning with a step interval of 0.02° and a scanning time of 2 s on each step. Lattice parameters of the solid-solutions were calculated with the LCR2 program[14] and further refined by the RIETAN program.[15]

Morphologies of the resultant powders were observed via field-emission scanning electron microscopy (FESEM, Model S-5000, Hitachi, Tokyo, Japan). Ultrasonically dispersed particles in ethanol are spread on the surface of a silicon plate. After drying at room temperature, osmium coating is performed before observation for better conductivity.

2.3. Sintering

Samples for sintering are isostatically consolidated under 300 MPa pressure. Densification behavior of the powder compact was monitored in air via dilatometry on a thermal-mechanical analyzer (Model TMA1700, Rigaku, Tokyo) using constant heating and cooling rates of 10 and 20 °C/min, respectively. Density of the powder compact, ρ, at any sintering temperature, is determined from the green density, ρ_0, and the measured linear shrinkage, $\Delta L/L_0$, using the following equation

$$\rho = \frac{\rho_0}{(1 - \Delta L/L_0)^3} \quad (1)$$

where L_0 is the initial sample length and, $\Delta L = L_0 - L$, where L is the instantaneous sample length. The green density of powder compact is calculated from its weight and geometric dimensions. Isothermal sintering was performed in a resistance furnace with a heating rate of 5 °C/min and a holding time of 2 h. Six sintering temperatures, 950, 1000, 1150, 1300, 1450, and 1550 °C, were used to vary grain size of the resultant ceramics. Microstructures of the sintered bodies were observed via FESEM from polished and thermally etched surfaces. Average grain sizes of the sintered bodies were determined by the linear interception method. The measured values were converted to the "true" grain sizes by multiplying with 1.56.

2.4. Electrical conductivity

Electrical conductivities of the sintered bodies were measured in air by the dc three-point method at temperatures

ranging from 400 to 700 °C, after Pt electrodes were applied to both sides of the sintered bodies (about ϕ 10 mm × 1.5 mm in size). The apparent activation energy for conduction was estimated from the Arrhenius plot.

3. Results and discussion

3.1. Powder synthesis and characterization

3.1.1. Composition of the precursor

In the carbonate coprecipitation method employing ammonium carbonate as the precipitant, the following equilibria were expected in the precipitation solution:

$$H_2O \Leftrightarrow H^+ + OH^- \quad (2)$$

$$(NH_4)_2CO_3 \Leftrightarrow 2NH_4^+ + CO_3^{2-} \quad (3)$$

$$NH_4^+ + OH^- \Leftrightarrow NH_4OH \Leftrightarrow H_2O + NH_3(g) \quad (4)$$

$$H^+ + CO_3^{2-} \Leftrightarrow HCO_3^- \quad (5)$$

and

$$H^+ + HCO_3^- \Leftrightarrow H_2CO_3 \Leftrightarrow H_2O + CO_2(g) \quad (6)$$

On the other hand, lanthanide cations are known to undergo weak hydration and slight hydrolysis in water to form complex species,

$$RE(H_2O)_n^{3+} + H_2O \Leftrightarrow [RE(OH)(H_2O)_{n-1}]^{2+} + H_3O^+ \quad (7)$$

where n is the coordination number of RE^{3+} cations.[16] During precipitation, the complexes formed in Eq. (7) reacted with the carbonate anions and other supporting ionic species generated through Eqs. (2)–(6) to form precipitates, and the final composition should ensure Ce^{3+} and RE^{3+} cations have the lowest solubilities in solution under the present precipitation conditions.

The as-dried precursor is amorphous to X-rays (will be shown later). Chemical analysis showed that the precursor contains ~41.5 wt.% of cerium, ~12 wt.% of dysprosium, ~1.3 wt.% of NH_4^+, and ~7.1 wt.% of carbon (from CO_3^{2-}). NO_3^- was not detected positively (detection limit: 0.01 wt.%), indicating that it is non-precipitating. Based upon the above results and considering molecular electrical neutrality, the precursor was assumed to be $(NH_4)_{0.25}CeDy_{0.25}(CO_3)_{2.0}\cdot 1.8H_2O$, where the molecular water was determined from the cerium or dysprosium content in the formulae.

3.1.2. Thermal decomposition and phase evolution of the precursor

Thermal behavior of the precursor powder has been investigated by DTA/TG, and the results were shown in Fig. 1. The decomposition of the precursor proceeds through three distinct stages. The first one, mainly occurring at temperatures up to ~183 °C, is due to the evaporation of the absorbed moisture and the release of ammonia and molecular water. The calculated weight loss (~13.1%) for this stage agree well with the value (~13.3%) revealed by TG ~183 °C. The second stage, occurring in the range ~183–346 °C, may correspond to the decomposition of rare-earth carbonate into oxycarbonate intermediates.[17] The weight loss at even higher temperatures (the third stage) is due to the further decomposition of the oxycarbonate to yield oxide. Complete decomposition is almost achieved at about 400 °C. The final weight loss (~32.58%) is also in accordance with that calculated (~35.2%) from the complete decomposition of $(NH_4)_{0.25}CeDy_{0.25}(CO_3)_{2.0}\cdot 1.8H_2O$, noticing the oxidation of Ce^{3+} to Ce^{4+} during heating.

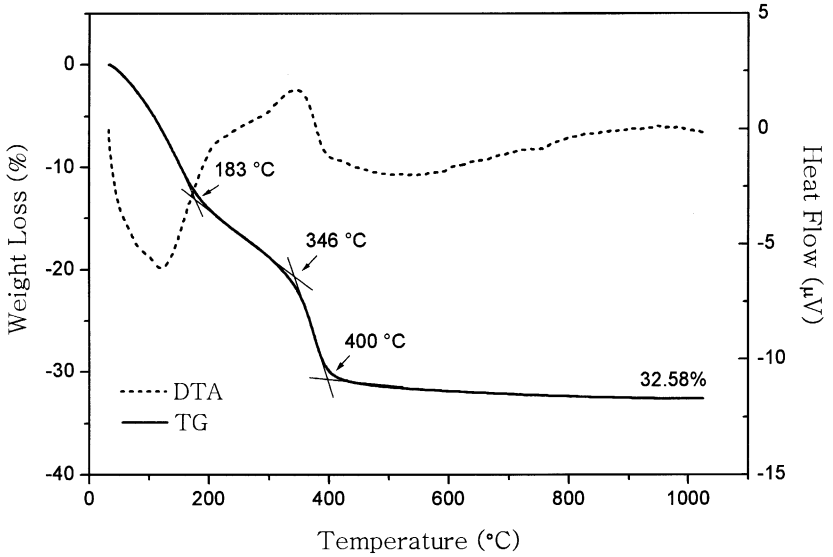

Fig. 1. DTA/TG curves of the as-dried 20DDC precursor. The data were taken in flowing air (200 ml/min) at a heating rate of 10 °C/min.

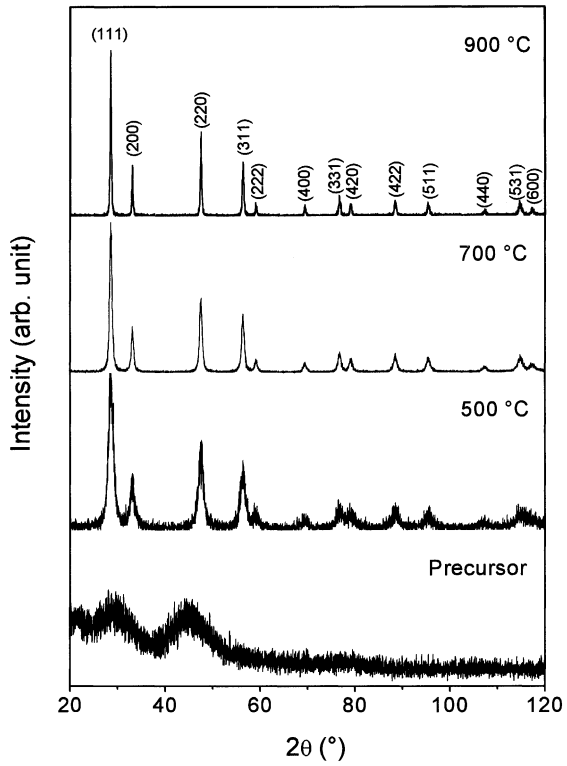

Fig. 2. XRD patterns of the 20DDC powders: precursor and its calcined products.

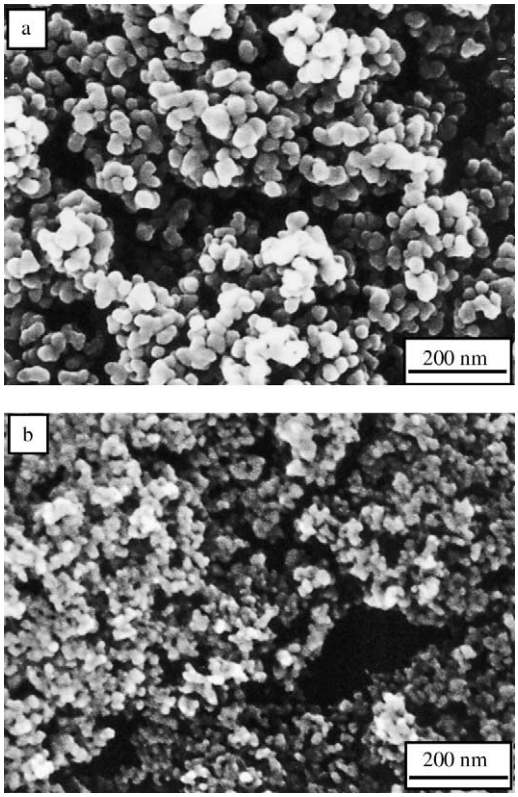

Fig. 3. FESEM micrographs showing morphologies of the 20DDC powders (a) the precursor and (b) the powder calcined at 700 °C for 2 h.

Fig. 2 shows XRD patterns of the 20DDC precursor and its calcination products. The as-dried precursor is essentially amorphous to X-rays. Crystallization of the powder occurs upon calcination at 500 °C, and major diffractions corresponding to the fluorite structure of CeO_2 (JCPDS: 34–394) have appeared. Continuous refinements in peak shapes and intensities were observed along with an increase in the calcination temperature, indicating crystallite growth. Crystalline phase corresponding to Dy_2O_3 was not detected, indicating the direct formation of solid solution. Lattice parameter of the 20DDC oxide calcined at 1000 °C was determined to be $a = 0.5404 \pm 0.0001$ nm, using the LCR2 program[14] and further refined by the RIETAN program[15] based on the Rietveld method. Apparently, Dy^{3+} doping induces a contraction in the unit cell of CeO_2 ($a = 0.541134$ (12) nm). The

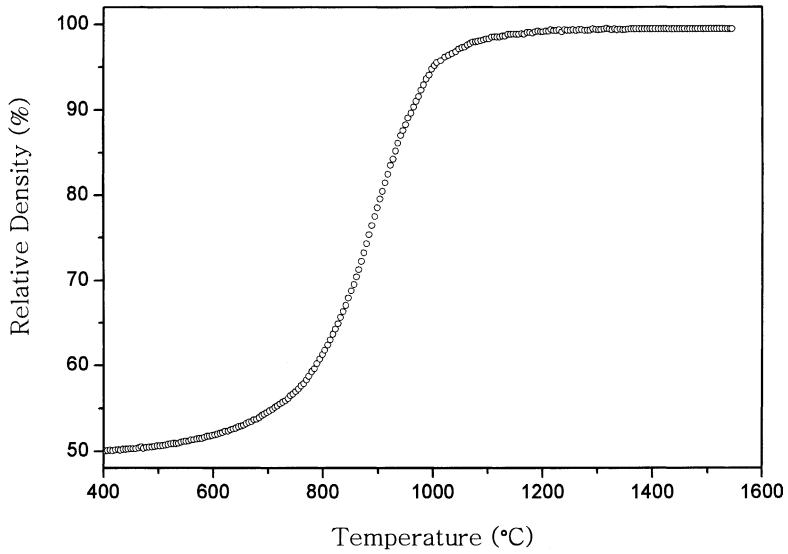

Fig. 4. Densification behavior of the 20DDC oxide. The heating and cooling rates are 10 and 20 °C/min, respectively.

powder calcined at 700 °C has an average crystallite size of ∼13.6 nm, as estimated for the Scherrer equation via X-ray broadening analysis performed on the (422) diffraction of the unit cell. This powder will later be used for sintering. The powders calcined at lower temperatures have smaller crystallite sizes, but they are difficult to consolidate into green bodies via dry pressing. Moreover, the powder compacts frequently crack upon heating, due to the stresses caused by rapid shrinkage.

3.1.3. Powder morphology

Fig. 3 shows particle morphologies of the precursor and the powder calcined at 700 °C. Apparently, the precursor is composed of rounded primary particles, which are only loosely agglomerated to form a porous network (Fig. 3a). The primary particles calcined up to 700 °C remain roughly spherical in morphology and have sizes of ∼10–15 nm in diameter (Fig. 3b). These size values are close to the crystallite size assayed from XRD (∼13.6 nm). Particles of the calcined powders are largely well dispersed, showing a morphology quite different from those produced via other wet-chemical routes, such as oxalate coprecipitation[9,10] and hydrothermal treatment.[12,13] Sintering behavior of a powder is mainly influenced by the particle size and the extent of aggregation. The ultrafine particle size and low agglomeration achieved by this carbonate coprecipitation method may imply good sinterability of the powder, as was confirmed by the sintering results shown below.

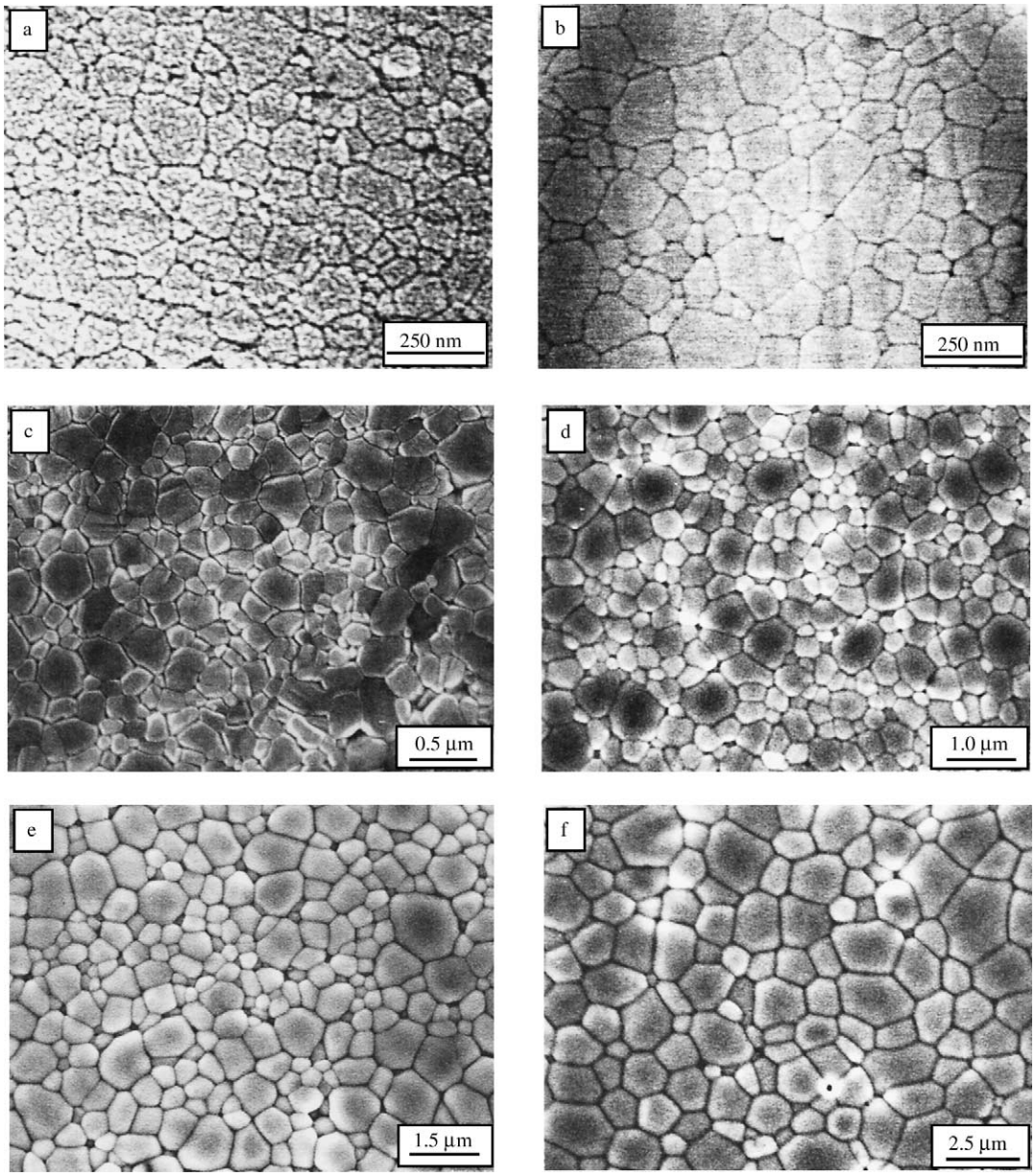

Fig. 5. FESEM micrographs showing microstructures of 20DDC densified for 2 h at (a) 950 °C, (b) 1000 °C, (c) 1150 °C, (d) 1300 °C, (e) 1450 °C and (d) 1550 °C.

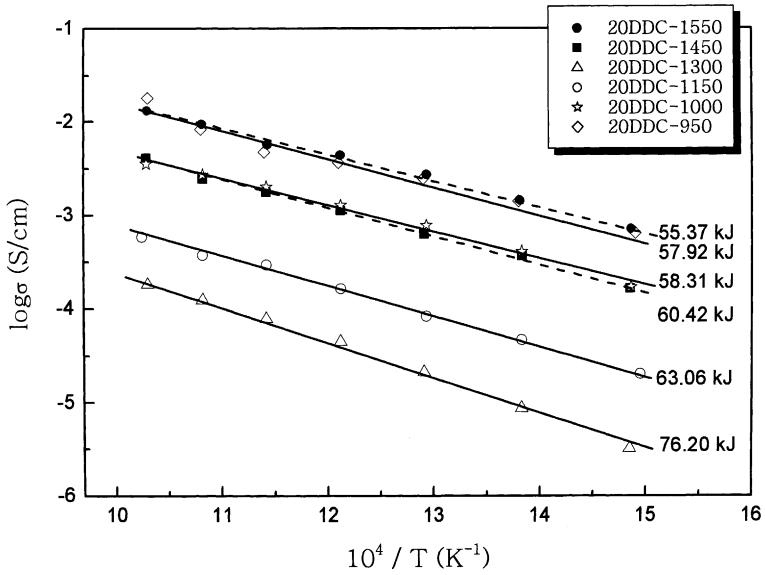

Fig. 6. Electrical conductivity of the densified 20DDC ceramics in air, as a function of temperature.

3.2. Densification behavior

Fig. 4 shows densification behavior of the 20DDC solid-solution powder calcined at 700 °C under a constant heating rate of 10 °C/min. Rapid shrinkage starts from the calcination temperature, and nearly full densification is reached at a very low temperature up to ~1100 °C.

The excellent sinterability of the powder was also demonstrated by the results of isothermal sintering: almost fully dense (>99% of the theoretical) 20DDC ceramic was made by pressureless sintering at 950 °C for 2 h. 20DDC ceramics with different grain sizes were then obtained by varying the sintering temperature up to 1550 °C, and microstructures of which were shown in Fig. 5.

3.3. Electrical conductivity

The electrical conductivities of 20DDC ceramics measured in air by the dc three-point method in the temperature range of 400–700 °C were given in Fig. 6, where the apparent activation energies were estimated from the Arrhenius equation: $\sigma T = \sigma_0 \exp(-E_a/RT)$. Linear relationship (with linear correlation coefficient >0.99) holds between $\lg \sigma T$ and $1/T$ for all the samples.

Fig. 7 shows the electrical conductivities measured at 700 °C and the apparent activation energies, as a function of the average grain size. A V-shape curve of conductivity was clearly seen, and the specimen with a mean grain size of ~0.24 μm showed the lowest conductivity (~$10^{-3.7}$ S/cm)

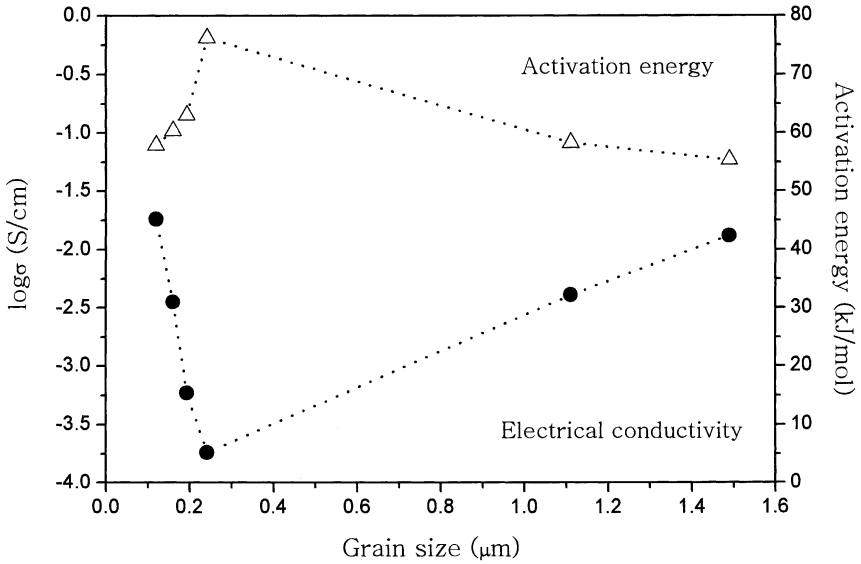

Fig. 7. Effects of grain size on the electrical conductivity and the apparent activation energy of 20DDC ceramics. The conductivities were measured at 700 °C in air.

and the highest activation energy (~76.2 kJ/mol). It is very interesting to notice the rapid and almost linear increase in conductivity at grain sizes below the critical value of ~0.24 μm. The specimen with the smallest grain size of ~0.12 μm (fabricated at 950 °C) exhibited a high conductivity of $10^{-1.74}$ S/cm, close to that of 10 mol% Sm_2O_3- or Gd_2O_3-doped ceria, the leading electrolytes among doped-ceria systems.[18,19] The improved conductivity at grain sizes above the critical value of ~0.24 μm may be understood from the brick layer model considering the decreased number of resistive grain boundaries. Similar phenomena was frequently observed in previous work,[6,20,21] for solid electrolytes with large grains (micron or above) and was explained similarly. The increased conductivity with decreasing grain size below the critical value, however, cannot be explained by the brick layer model, though the phenomenon was also encountered in other materials systems. Nanocrystalline $(RE_2O_3)_{0.08}(ZrO_2)_{0.92}$ (RE = Sc, Y)[22] was reported to show ionic conductivities one order of magnitude higher than those of micron-grained materials, and the reason was ascribed to the decrease of grain boundary resistance related to "interfacial effects." Tian and Chan[23] studied the conductivity and microstructure of Y_2O_3-doped CeO_2 and similarly got a higher conductivity at a lower sintering temperature. It should be noted that, due to the poor reactivity of their powders, they did not obtain dense sintered bodies at temperatures below 1500 °C. The increased conductivity at grain size below ~0.24 μm may be understood from the following aspects, as suggested by Tian and Chan: (1) the sample sintered at a lower temperature has lower impurity concentration, fewer precipitates, and less continuous blocking layers at grain boundaries, resulting from the smaller grain size and the larger grain boundary area; (2) the grain boundaries have lower segregation of solutes and less well developed space charge regions, due to the smaller grain size and the lower mobility of cations at lower temperatures, respectively. Grain boundary conduction behavior would be helpful to verify the above mechanisms and to understand the improved conductivity at a smaller grain size below the critical value of ~0.24 μm. We tried, but failed, to separate the grain boundary conductivity from the bulk by the ac impedance method, due to the severe superposition of the semicircles arising from the fine grain sizes. An alternative is careful microstructural analysis, especially on the grain boundary regions, and the work is underway.

4. Conclusions

10 mol% Dy_2O_3-doped ceria has been synthesized via a carbonate coprecipitation method using ammonium carbonate as precipitant and nitrates as starting salts. The thus-derived powders exhibit excellent sinterability and can be highly densified at a very low temperature of 950 °C. The relationship between electrical conductivity and grain size was investigated in a regime of 0.12–1.5 μm, and the conductivity exhibits a V-shape curve against the grain size. A minimum conductivity was observed in the specimen sintered at 1300 °C and with an average grain size ~0.24 μm.

References

1. Steel, B. C. H. and Heinzel, A., Materials for fuel-cell technologies. *Nature* 2001, **414**, 345–352.
2. Haile, S. M., Fuel cell materials and components. *Acta Mater* 2003, **51**, 5981–6000.
3. Etsell, T. H. and Flengas, S. N., The electrical properties of solid oxide electrolytes. *Chem. Rev.* 1970, **70**, 339–376.
4. Bonanos, N., Steele, B. C. H. and Butler, E. P., Applications of impedance spectroscopy. In *Impedance Spectroscopy*, ed. J. R. Macdonald. Wiley, New York, 1987, Chapter 4, p. 191.
5. Verkerk, M. J., Middelhuis, B. J. and Burggraaf, A. J., Effect of grain boundaries on the conductivity of high-purity ZrO_2—Y_2O_3 ceramics. *Solid State Ionics* 1982, **6**, 159–170.
6. Christie, G. M. and van Berkel, F. P. F., Microstructure—ionic conductivity relationships in ceria-gadolinia electrolytes. *Solid State Ionics* 1996, **83**, 17–27.
7. Kudo, T. and Obayashi, H., Oxygen ion conduction of the fluorite-type $Ce_{1-x}Ln_xO_{2-x/2}$ (Ln = Lanthanoid Element). *J. Electrochem. Soc.* 1975, **122**, 142–147.
8. Yahiro, H., Eguchi, K. and Arai, H., Electrical properties and reducibilities of ceria-rare earth oxide systems and their application to solid oxide fuel cell. *Solid State Ionics* 1989, **36**, 71–75.
9. Hertle, J. V., Horita, T., Kawada, T., Sakai, N., Yokokawa, H. and Dokiya, M., Oxalate coprecipitation of doped ceria powder for tape casting. *Ceram. Int.* 1998, **24**, 229–241.
10. Higashi, K., Sonoda, K., Ono, H., Sameshita, S. and Hirata, Y., Synthesis and sintering of rare-earth-doped ceria powder by oxalate coprecipitation method. *J. Mater. Res.* 1999, **14**, 957–967.
11. Huang, K., Feng, M. and Goodenough, J. B., Synthesis and electrical properties of dense $Ce_{0.9}Gd_{0.1}O_{1.95}$ ceramics. *J. Am. Ceram. Soc.* 1998, **81**, 357–362.
12. Yamashita, K., Ramanujachary, K. V. and Greenblatt, M., Hydrothermal synthesis and low temperature conduction properties of substituted ceria ceramics. *Solid State Ionics* 1995, **81**, 53–60.
13. Huang, W., Shuk, P. and Greenblatt, M., Hydrothermal synthesis and properties of $Ce_{1-x}Sm_xO_{2-x/2}$ and $Ce_{1-x}Ca_xO_{2-x}$ solid solutions. *Chem. Mater.* 1997, **9**, 2240–2245.
14. Williams, D. E., *Tech. Rept. No. IS-1052*. Ames Laboratory, U.S.D.O.E., Iowa State University, Ames, IA, 1964.
15. Izumi, F. and Ikeda, T., A Rietveld-analysis program RIETAN-98 and its applications to zeolites. *Mater. Sci. Forum* 2000, **198**, 321–350.
16. Topp, N. E., *The Chemistry of Rare-Earth Elements*. Elsevier, Amsterdam, 1965.
17. Moscardini, L., Giolito, I. and Ionashiro, M., Thermal decomposition of the hydrated basic carbonates of lanthanides and yttrium. *Thermochim. Acta* 1989, **137**, 310–319.
18. Dirstine, R. T., Blumenthal, R. N. and Kuech, T. F., Ionic conductivity of calcia, yttria, and rare earth-doped cerium dioxide. *J. Eletrochem. Soc.* 1979, **126**, 264–269.
19. Eguchi, K., Setoguchi, T., Inoue, T. and Arai, H., Electrical properties of ceria-based oxides and their application to solid oxide fuel cells. *Solid State Ionics* 1992, **52**, 165–172.

20. Gerhardt, R., Norwick, A. S., Mochel, M. E. and Dumler, I., Grain-boundary effect in ceria doped with trivalent cations. I. Electrical measurements. *J. Am. Ceram. Soc.* 1986, **69**, 641–646.
21. Wang, D. Y. and Norwick, A. S., The "grain-boundary effect" in doped ceria electrolytes. *J. Solid State Chem.* 1980, **35**, 325–333.
22. Zhang, Y. W., Jin, S., Yang, Y., Li, G. B., Tian, S. J., Jia, J. T. *et al.*, Electrical conductivity enhancement in nanocrystalline $(RE_2O_3)_{0.08}(ZrO_2)_{0.92}$ (RE = Sc, Y) thin films. *Appl. Phys. Lett.* 2000, **77**, 3409–3411.
23. Tian, C. and Chan, S.-W., Ionic conductivities, sintering temperatures and microstructures of bulk ceramic CeO_2 doped with Y_2O_3. *Solid State Ionics* 2000, **134**, 89–102.